Molecular Engineering of Elastic and Strong Supertough Polyurethanes

ARTICLE *in* MACROMOLECULES · APRIL 2012

Impact Factor: 5.8 · DOI: 10.1021/ma300397e

Macromolecules

Article

pubs.acs.org/Macromolecules

Molecular Engineering of Elastic and Strong Supertough Polyurethanes

Borja Fernández-d'Arlas, Jose A. Ramos, Ainara Saralegi, Marian Corcuera, Iñaki Mondragon, and Arantxa Eceiza*

Grupo "Materiales + Tecnologías" (GMT), Department of Chemical and Environmental Engineering, Polytechnic School, University of the Basque Country (UPV/EHU), Pza. Europa 1, 20018 Donostia-San Sebastián, Spain

Supporting Information

ABSTRACT: Spider silk is an icon of supertough energy absorbing polymeric material which its macromolecular multiblock composition has been attributed to be responsible for such remarkable properties. As in spider silk, polyurethanes can be synthesized with two distinct block which can differ in nature, combining properties like deformability and relatively high strengths. Here we synthesized and studied four different block polyurethanes with two different soft segments (SS) and two different hard segments (HS), with the aim of discovering the best molecular architecture to develop best mechanical performance after macromolecular alignment. The difference between soft segments is the crystalline nature, one in the rubbery state ($T_{g,SS} < T_{room}$) and the other in the semicrystalline state at room temperature ($T_{room} < T_{m,SS}$). In parallel one hard segment was amorphous in the glassy state ($T_{room} < T_{g,HS}$) and the other semicrystalline ($T_{g,HS} < T_{room} < T_{m,HS}$). Results indicate that polyurethane with crystalline soft segments produce stronger materials after drawing than polyurethanes with rubbery soft segments, but the most exciting finding is the influence that hard segment has on the mechanical performance of predrawn materials, having polyurethanes prepared with semicrystalline hard segments more capability to undergo macromolecular alignment than materials with glassy segments, developing stiffer, stronger, and tougher materials.

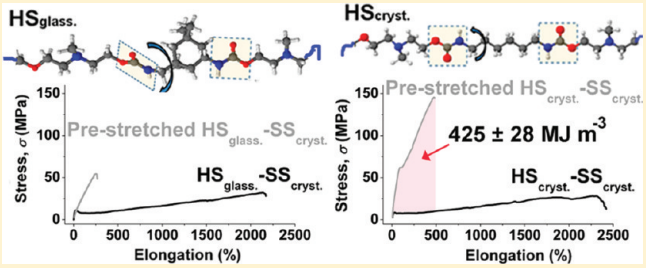

INTRODUCTION

Extraordinary mechanical properties of spider silk[1−5] have inspired material scientists to undertake research on a new field of science pursuing supertough materials based on molecular engineering and understanding of fracture and toughening mechanisms underlying on spider silk molecular structure[6,7] and materials.[8] Simultaneously, achievement of highly elastic materials, reversibly highly deformable, but with high yield and tensile stresses[9,10] has resulted in an equally challenging goal. In the last years researches have concluded that spider silk's combination of extensibility and strength under tension arises from the copolymeric nature of the silk polypeptidic protein sequences consisting on crystalline, alanine-rich segments in antiparallel β-sheet configuration linked to glycine-rich amorphous domains.[1,7] In addition, the orientated chain anisotropy caused by fiber drawing has been shown to be an equally important factor to that of the chemical composition.[11]

Development of supertough, energy absorbing, materials has been traditionally pursued by either improving the deformability of stiff and strong materials, for example by adding block copolymers,[12] or by strengthening soft and very deformable materials with the inclusion of fibers[9] or nanoparticles.[13] Nevertheless, natural silks, which comprise the toughest materials known to date,[5] are composed of single polymeric molecules not blended with any other nonpolypeptidic structures. Great efforts have been put into understanding structure-properties relationships of spider and worm silks.[14] Even attempts to synthesize *in vivo* silks by genetic engineering of goats mammalian cells[15] have drawn the attention of materials scientists, but not managed to equal natural silk fibers mechanical performance, despite the complexity of the procedure. On the basis of the idea that astonishing mechanical performance of silk relays on its block copolymeric nature of its polypeptidic protein chains and that these are oriented at spinning developing great stiffness and strength,[1,11] we envisioned the idea of creating spider silk like supertough materials supported on our experience on engineering of block polyurethanes.[9,16,17] Here we explore thermoplastic polyurethane copolymers with different block architecture as possible candidates to become industrially scalable synthetic mimics of spider silk like materials. Based on the design possibilities block polyurethanes (PU) offer and on experimental results, we discuss the chain architecture requirements to achieve a strong and highly deformable supertough material.

Polyurethane elastomers share with silks its copolymeric nature consisting on hard segments (HS) linked to soft segments (SS) in an alternative fashion. Thermodynamic incompatibility between HS and SS as well as steric and

Received: February 25, 2012
Revised: April 4, 2012
Published: April 13, 2012

physicochemical properties of each of the segments[17] lead to certain microphase separated structures, consisting on HS nanocylinders of about 5−25 nm dispersed within a SS matrix.[16] This terminology of HS and SS comes from the idea that in typical polyurethane elastomers the HS are semicrystalline in nature, in the vast majority of the cases with glass-transition and melting temperatures well above ambient temperature ($T_{room} < T_{g,\ HS} < T_{m,\ HS}$) while typically SS are usually in the rubbery state at room temperature with both the glass transition and melting temperatures well below room temperature ($T_{g,\ SS} < T_{m,\ SS} < T_{room}$).[13,17] On the basis of these considerations, in this work we wanted to modestly summarize in four PU cases, the possible situations in which each of the HS and SS display either amorphous (glassy-rubbery) or semicrystalline states at room temperature, and study its performance after orienting their molecules along the stretching axis, as in a fashion of spider silk spinning.

EXPERIMENTAL SECTION

Polyurethanes Synthesis. PU synthesis was realized via two shot polymerization method, in a four necked round-bottom reactor provided with a mechanical stirrer. The molecular weights of the polyols were 2020 and 1980 g mol^{-1} for the $SS_{rubb.}$ and $SS_{cryst.}$, respectively, as measured by backward hydroxyl titration. The polyols were made react with the diisocyanates under N_2 atmosphere. For 1,6-hexamethylene diisocyanate (HDI, Bayer) based PU the reaction time and temperature at this stage were 5 h and 100 °C according to previous kinetic studies.[18] The reaction with 5-isocyanato-1-(isocyanatomethyl)-1,3,3-trimethyl-cyclohexane (also known as Isophorone diisocyanate, IPDI, Bayer) was undergone for 24 h at 100 °C due to the lower reactivity of IPDI. The chain extender MDEA (Aldrich), was added at the end of this first stage and the mixture was stirred vigorously for 10 min and then poured to polytetrafluorethylene (PTFE) coated molds and pressed at 50 bar and 100 °C for 10 h. Hard segments based on IPDI were designated as $HS_{glass.}$ and hard segments based on HDI as $HS_{cryst.}$.The stoichiometric ratio diisocyanate:-poyol:MDEA was in all cases 3:1:2. Molecular weight distributions were calculated by size exclusion chromatography. All polyurethanes presented comparable molecular weights (see Table 1).

Table 1. Molecular Weight Distributions of Polyurethanes[a]

polyurethane	M_w	M_w/M_n	$M_{w,max}$
$HS_{glass.}$-$SS_{rubb.}$	47 520	2.1	323 496
$HS_{glass.}$-$SS_{cryst.}$	44 120	2.2	338 573
$HS_{cryst.}$-$SS_{rubb.}$	54 570	1.5	258 506
$HS_{cryst.}$-$SS_{cryst.}$	50 090	1.4	344 254

[a] M_w, weight average molecular weight; M_w/M_n, polydispersity index; $M_{w,max.}$, maximum M_w for longest chains in the samples.

Size Exclusion Chromatography (SEC). The molecular weights and molecular weight distributions were analyzed by size exclusion chromatography with a PerkinElmer chromatograph equipped with a binary pump and a refractive-index detector. The mobile phase was tetrahydrofuran (THF), and the separation was carried out with three columns packed with particle gels with different nominal pore sizes. Elution rate was of 1 mL min^{-1} at 30 °C. The samples were dissolved to 1 wt % in THF. The molecular weights and molecular weight distributions were based on a calibration curve with monodisperse polystyrene standards.

Differential Scanning Calorimetry (DSC). Differential scanning calorimetry (DSC) analysis between −60 and 250 °C was performed on a Mettler Toledo calorimeter at heating rates of 20 °C min^{-1} under constant N_2 flow. Stretched samples were pre-drawn for 10 min just before being analysed.

Polarized Optical Microscope (POM) and Atomic Force Microscope (AFM) Morphology Monitoring. Samples for POM studies were prepared by casting PU (50 mg mL^{-1}, THF) solutions into PTFE molds and controlled evaporation to produce films which ranged from 100 μm (low magnification images) to 10−50 μm for high magnification images showing spherullitic structures. For deforming the samples and holding them into microscopes set-ups a small stretching device consisting on two clamps and a screw guide with submillimetric precision to control strain, was designed and built (Suguz, Donostia-San Sebastián, Spain). AFM images were taken in the tapping mode in air at room temperature at different strains leaving to relax the samples at each strain for at least 10 min. The used aquipment was a Nanoscope IV, Dimension 3100 from Digital Instruments.

Dynamic Fourier Transformed Infrared Spectroscopy (FTIR). Samples for FTIR studies were prepared by casting PU (50 mg mL^{-1},THF) solutions into PTFE molds and controlled evaporation to produce films with thicknesses between 10 and 50 μm. Spectra at different strains were recorded on the transmission mode on a Nicolet-Nexus-FTIR spectrometer and obtained by averaging 20 scans between 4000 and 400 cm^{-1} with a resolution of 2 cm^{-1} after leaving relax the samples at least 10 min at measuring strains.

Materials Prestretching and Mechanical Testing. Samples for tensile testing were die cut from hot pressed films, prepared by heating up to 180 °C for 5 min with 1 ton of pressure, and slow cooling to 30 °C. Mechanical properties of films casted from tetrahydrofuran and hot-pressed films resulted to be similar. Cross-head deformation speed was of 100 mm min^{-1} for all samples. The prestretching experiments consisting on deforming the samples up to ∼1500% for 10 min. During that time stress were recorded at 0.5, 1, 2, 3, 5, 7, and 10 min for the stress-relaxation studies. The prestretched samples thicknesses and widths were measured again after the prestretching and then clamped in such a way that only the predrawn material suffered the tensile stress.

Molecular Models. Molecular models were drawn using ACD/ChemSketch (Freeware version) from ACD/Labs.

RESULTS AND DISCUSSION

The four PU were synthesized in our lab by the common two-shot polymerization method[17] and temperatures and times were chosen according to previous tests so to achieve high molecular weight PU macromolecules, as can be observed by size exclusion chromatography data gathered in Table 1. As seen in Table 1 the M_w was slightly lower for polyurethanes based on isophorone diisocyanate, IPDI, (those with $HS_{glass.}$) than those based on 1,6-hexamethylene diisocyanate, HDI, (those with $HS_{cryst.}$). This fact is related to the lower reactivity of IPDI respect to HDI. The polydispertity was also higher for IPDI-based polyurethanes and this is also related to the lower reactivity of IPDI respect to HDI. In any case M_w of polyurethanes were close enough to associate the differences observed in this work merely to polyurethanes segments architecture variations.

The chemical structure of the polyurethanes is sketched in Figure 1a. The changing parameters between different PU were the diisocyanate and the polyol employed. The diisocyanates were either HDI or IPDI. The SS employed were either a castor oil derived polyester diol consisting on sebacic acid copolymerized with 1,4-butanediol ($SS_{cryst.}$) or a poly(ester-*co*-carbonate) diol consisting on 1,6-hexamethylene carbonate copolymerized with caprolactone ($SS_{rubb.}$). The subscripts cryst. and rubb. describe the morphology state of each SS at room temperature, crystalline ($T_{room} < T_{m,\ SS}$) and rubbery ($T_{g,\ SS} < T_{m,\ SS} < T_{room}$), respectively. The chain extender was in all cases *N*-methyl-diethanolamine (MDEA). Hard segments formed by MDEA and HDI were semicrystalline ($HS_{cryst.}$) with $T_{g,HS} > T_{room}$ and a $T_{m,\ HS} < T_{room}$, while hard segments formed by MDEA and IPDI were amorphous at the glassy state ($HS_{glass.}$)

dx.doi.org/10.1021/ma300397e | Macromolecules 2012, 45, 3436−3443

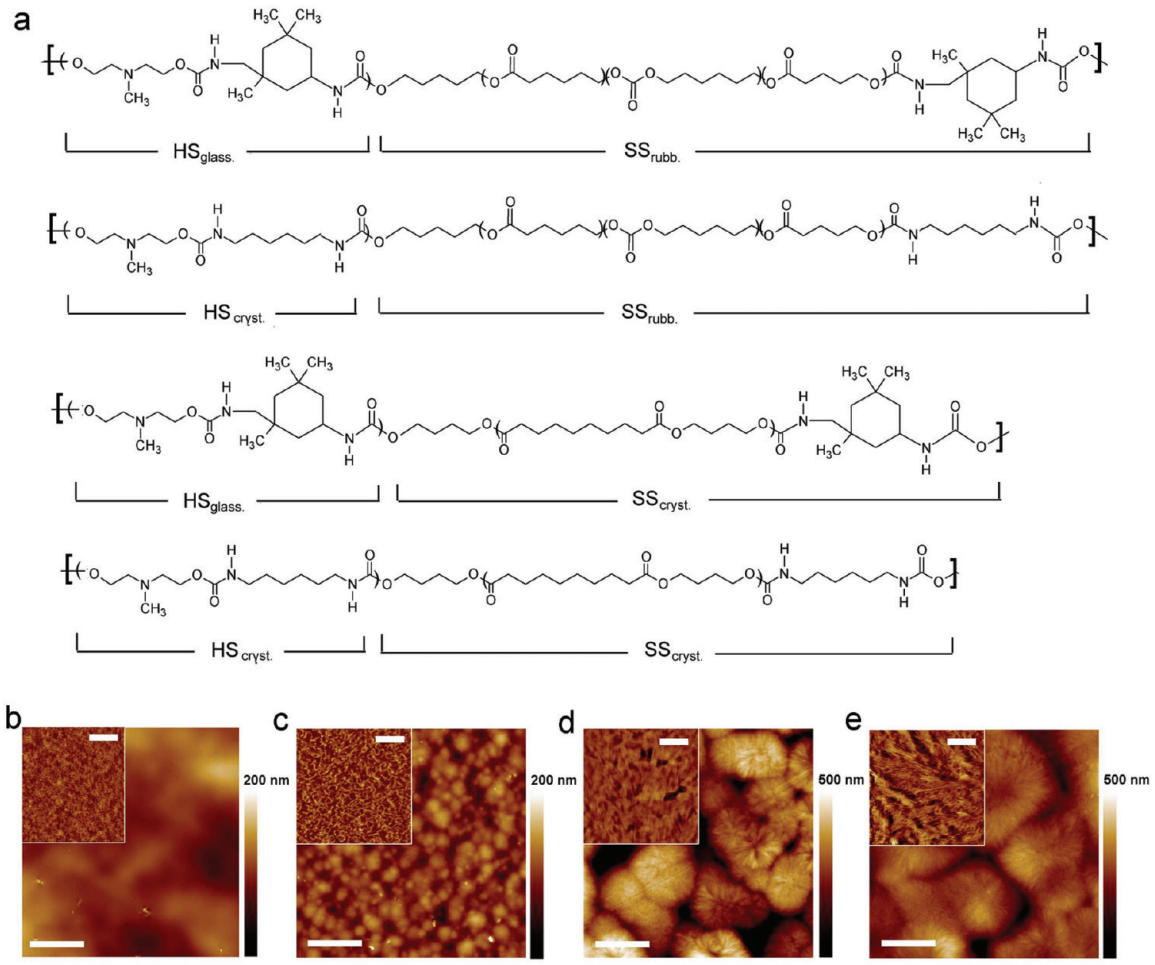

Figure 1. (a) Sketches of polyurethane chain architecture and materials morphology as observed by AFM of (b) $HS_{glass.}$-$SS_{rubb.}$, (c) $HS_{cryst.}$-$SS_{rubb.}$, (d) $HS_{glass.}$-$SS_{cryst.}$, and (e) $HS_{cryst.}$-$SS_{cryst.}$. The height images sizes are 40 μm × 40 μm scan area with a scale bar of 10 μm. The inset images are 1 μm × 1 μm phase images with scale bars of 250 nm.

with $T_{g,\ HS} > T_{room}$. The morphology of each of the polyurethane casted from solution (see Experimental Section) as analyzed by atomic force microscopy (AFM) is included nearby each structure in Figure 1b–e. In the large scale height images it can be observed the increasing tendency to form bigger spherullites as the overall proportion of crystalline fraction is increased from Figure 1b to Figure 1e. In the small range phase images, it is seen that the microphase morphology varies from nanometric scale hard globules (related to HS_{glass} domains) dispersed in the amorphous $SS_{rubb.}$ matrix, in Figure 1b, to worm-like nanocrystals consisting on partially crystallized $HS_{cryst.}$ nanodomains dispersed in $SS_{rubb.}$ matrix, in Figure 1c. Comparing images in Figure 1d and Figure 1e it is seen that both materials develop large lamellas due to the soft segment crystallizing tendency, although in Figure 1e larger, brighter and more defined lamellas are observed due to the higher tendency of the $HS_{cryst.}$ to crystallize than $HS_{glass.}$ (see Figure 2).

Macromolecular alignment was attained by prestretching the samples at 1500% strain for 10 min. At this time stress relaxation with time leveled off down to a quasi-equilibrium stress value, or very slow decrease with time (see Supplementary Figure §1), indicating that at this time most of the polymer chains reached minimum energy conformations and organization for the given strain. Although molecular processes occurring when drawing are complex in PU elastomers it is generalized that arrangements and reorientation of hard domains and alignment and crystallization of soft domains take part.[19,20] Morphology was also studied by thermal analysis (DSC) of nonstretched and stretched samples. Figure 2 show thermograms of non stretched and stretched specimens. Stretching $HS_{glass.}$-SS_{rubb} leads to no noticeable morphological changes detected by DSC. This can be attributed to the amorphous nature of both blocks which cannot promote supramolecular organization upon stretching while, stretching $HS_{cryst.}$-$SS_{rubb.}$ leads to supramolecular organization of $HS_{cryst.}$ segments into an ordered phase with melting transition around 225 °C. Also a mechanically driven phase mixing between $HS_{cryst.}$ and $SS_{rubb.}$ produced an increase of $SS_{rubb.}$ phase glass transition temperature about 3 °C.

Stretching $HS_{glass.}$-$SS_{cryst.}$ leads to $SS_{cryst.}$ strain induced crystallization, as can be observed by the increased area of the $SS_{cryst.}$ phase melting transition around 50 °C. No noticeable changes in transition associated with $HS_{glass.}$ were observed. The increase of the lower melting peak phase enthalpy in the melting transition associated with soft segments, when stretching, suggests a favored formation of the less ordered structure appreciated as a low temperature shoulder peak in both nonstretched and stretched materials. Stretching of $HS_{cryst.}$-$SS_{cryst.}$ produces both a $SS_{cryst.}$ and $HS_{cryst.}$

dx.doi.org/10.1021/ma300397e | Macromolecules 2012, 45, 3436–3443

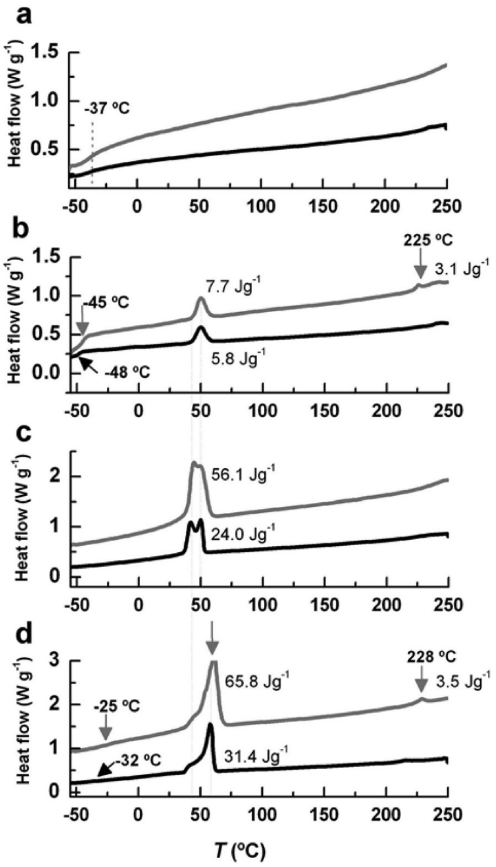

Figure 2. Differential scanning calorimetry (DSC) of nonstretched (black) and prestretched samples to 1500% for 10 min (gray) of (a) $HS_{glass.}$-$SS_{rubb.}$, (b) $HS_{cryst.}$-$SS_{rubb.}$, (c) $HS_{glass.}$-$SS_{cryst.}$ and (d) $HS_{cryst.}$-$SS_{cryst.}$.

ordered phases increase in melting enthalpies, consequence of a better alignment of both segments along the strain direction.

Under the cross-polarized microscope it is observed a change from spherulitic structure to a pure fibrous structure as samples are stretched, more clearly seen in samples with crystallizable segments (Figure 3a and Supplementary Figure §2). Both morphologies contain high level of ordered substructures responsible of birefringence, but with obvious differences in higher levels of macromolecular organization. In the case of completely amorphous polyurethane ($HS_{glass.}$-$SS_{rubb.}$) no brightness contrast is observed after yield, what can be related to the disruption of the enthalpically driven low energy globular structures of $HS_{glass.}$ attained by the slow cooling at processing, and incapability of both segments to undergone self-organization into high level ordered structures with capability to produce optical interferences.

Evolution of morphology with strain at lower scales was also monitored by AFM with samples supported at different strains with a home-designed extensometer (see Experimental Section). Figure 3b,c present AFM phase images of $HS_{cryst.}$-$SS_{cryst.}$ and $HS_{glass.}$-$SS_{cryst.}$ nanostructure at 600% of deformation. While in the case of $HS_{cryst.}$-$SS_{cryst.}$ a clear nanofibrous morphology with fibers separated by ~50 nm (see inset of Figure 3b) the $HS_{glass.}$-$SS_{cryst.}$ strained up to 600% did not present a fibrous morphology at the nanoscale (Figure 3c). This corresponds to a lack in ordering upon drawing due to the $HS_{glass.}$ restricted mobility arising from the intrinsic cyclic nature of IPDI ring and for its bulky methyl groups which hinder crystallization mechanisms.[21] Both the microstructure and nanostructure seemed to present a fractal like fibrous structure, which in addition evolves in an opposite direction producing wider and more separated micropits at the micro level and thinner and more packed fibrils at the nano level (see Supplementary Figure §3). Changes at the micro level are related to spherullite disruption and orientation of the lamellae along the strain direction,[22] and to the collapse of adjacent

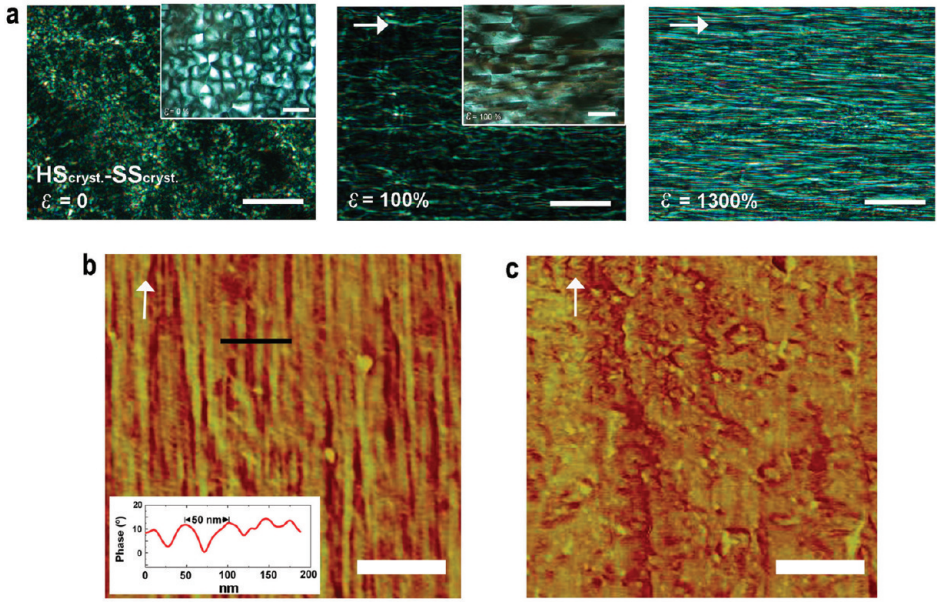

Figure 3. Morphology variation with strain. (a) Cross-polarized optical microscopy images of $HS_{cryst.}$-$SS_{cryst.}$ morphology variation with the indicated strain. The scale bars correspond to 40 μm and to 20 μm for the inset images. (b) AFM 1 μm × 1 μm phase image of the $HS_{cryst.}$-$SS_{cryst.}$ material at 600% strain, indicating the phase profile for a specific set of fibrils indicated with a black line. (c) AFM 1 μm × 1 μm phase image of $HS_{glass.}$-SS_{cryst} material at 600% for comparison with "b". The scale bars of the AFM images are of 250 nm. White arrows indicate strain direction.

dx.doi.org/10.1021/ma300397e | *Macromolecules* 2012, 45, 3436–3443

spherullites due to normal forces arising perpendicular to strain direction. Lack of fibrous nano level order was observed in $HS_{glass.}$-$SS_{cryst.}$ with small range phase AFM images at different elongations.

Molecular conformation evolution with strain was monitored by dynamic Fourier-transform infrared spectroscopy (FTIR) (see Experimental Section). Figure 4a,b show urethane N−H

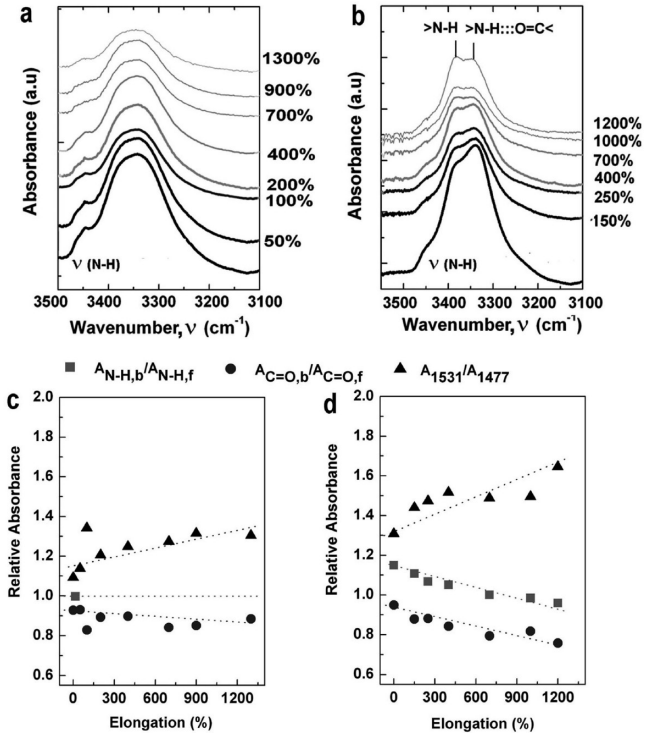

Figure 4. Dynamic FTIR analysis of hydrogen bonding changes with strain. FTIR absorption region of N−H stretching bands for (a) $HS_{glass.}$-$SS_{cryst.}$ and (b) $HS_{cryst.}$-$SS_{cryst.}$ at different strains. Relative absorbancies between the indicated functional groups at different strains for (c) $HS_{glass.}$-$SS_{cryst.}$ and (d) $HS_{cryst.}$-$SS_{cryst.}$.

stretching region of $HS_{glass.}$-$SS_{cryst.}$ and $HS_{cryst.}$-$SS_{cryst.}$, respectively. It is seen that while the $HS_{glass.}$-$SS_{cryst.}$ present a single wide peak which do not vary in shape with strain, $HS_{crys.}$-$SS_{cryst.}$ presents a two peak absorption band typical from partially hydrogen bonded amides and urethanes.[17] In addition, in the later, the relation between hydrogen bonded N−H peak at 3320 cm^{-1} and non-hydrogen bonded N−H peak varies with strain, with a tendency to increase the non-hydrogen bonded N−H absorbance over the hydrogen bonded. In the carbonyl (C═O) region, both the $HS_{glass.}$-$SS_{cryst.}$ and $HS_{cryst.}$-$SS_{cryst.}$ PUs developed higher absorbancies of non-hydrogen bonded carbonyl stretching peak at 1730 cm^{-1} with increasing strain. Parts c and d of Figure 4 present the ratio of absorbancies between different peaks at different strains. For both PUs the ratio between hydrogen bonded carbonyls and non-hydrogen bonded carbonyls, $A_{C=O,b}/A_{C=O,f}$ trends to decrease what, considering molar absorptivities of different species vary in the same ratio with strain, means an overall disruption of hydrogen bonded carbonyls. The ratio between hydrogen bonded and non hydrogen bonded N−H, $A_{N-H,b}/A_{N-H,f}$ only trends to decrease with strain for the $HS_{cryst.}$-$SS_{cryst.}$ PU what indicates N−H group is not as much involved in macromolecular conformation changes with strain in $HS_{glass.}$-$SS_{cryst.}$ as in $HS_{cryst.}$-$SS_{cryst.}$. The tendency to hydrogen bonding disruption upon stretching has also been reported by other researchers, and has been attributed to either lamellae disruption[19] and secondary structures intramolecular hydrogen bonding breakage.[23] The ratio between bending bands of N−H at 1531 cm^{-1} and C−H at 1475 cm^{-1} is higher for $HS_{cryst.}$-$SS_{cryst.}$ than $HS_{glass.}$-$SS_{cryst.}$ due to hard segment composition differences, but increase of the ratio also appears higher, corresponding again to a more profound conformational change of this structure. Band peaks position, which are associated with functional groups bonds energetic levels[24] can be shifted toward different position depending on chemical environment[25] or mechanical stress.[24] In Figure 5a−c, we see that specific peaks of N−H stretching

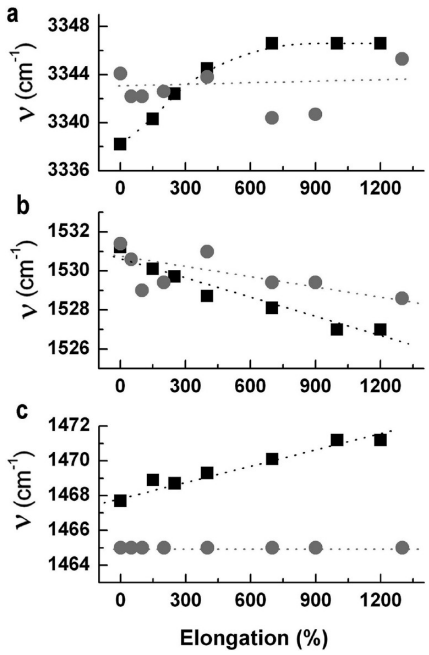

Figure 5. Wavenumber (ν) frequency shifts of peaks from stretching and bending absorption bands of (a) N−H stretching, (b) N−H bending and (c) C−H bending functional groups for both $HS_{glass.}$-$SS_{cryst.}$ (gray circles) and $HS_{cryst.}$-$SS_{cryst.}$ (black squares).

and bending and C−H bending are shifted with strain more pronouncedly for $HS_{cryst.}$-$SS_{cryst.}$. Corresponding these absorption bands to groups embedded within the PU hard segments it is concluded that hard segments of $HS_{cryst.}$ segments participate more on PU overall deformation than $HS_{glass.}$. Figure 6 sketches the above conclusions for spherullitic lamella disruption by the action of the stress on both $HS_{cryst.}$-$SS_{cryst.}$ and $HS_{glass.}$-$SS_{cryst.}$ giving ordered and less ordered fibrils, respectively. It also presents the molecular most stable conformation of both $HS_{glass.}$ and $HS_{cryst.}$. It is observed that urethane groups (OCONH) of $HS_{cryst.}$ repetitive units lay on very similar planes to respect to the chain axis, while in the case of $HS_{glass.}$ OCONH groups lay on very different planes, which obviously restrict inter chain molecular associations.

Tensile mechanical properties of non-prestretched PU were strongly dependent on molecular composition (Figure 7). Materials mechanical properties are resumed in Table 2. The materials with rubbery SS presented low elastic modulus, E, and yield stresses, σ_y, and among them the strength was higher for the $HS_{cryst.}$-$SS_{rubb.}$ because of the partial crystallinity of the HS, which holds the structure via thermally reversible pseudocross-

dx.doi.org/10.1021/ma300397e | Macromolecules 2012, 45, 3436−3443

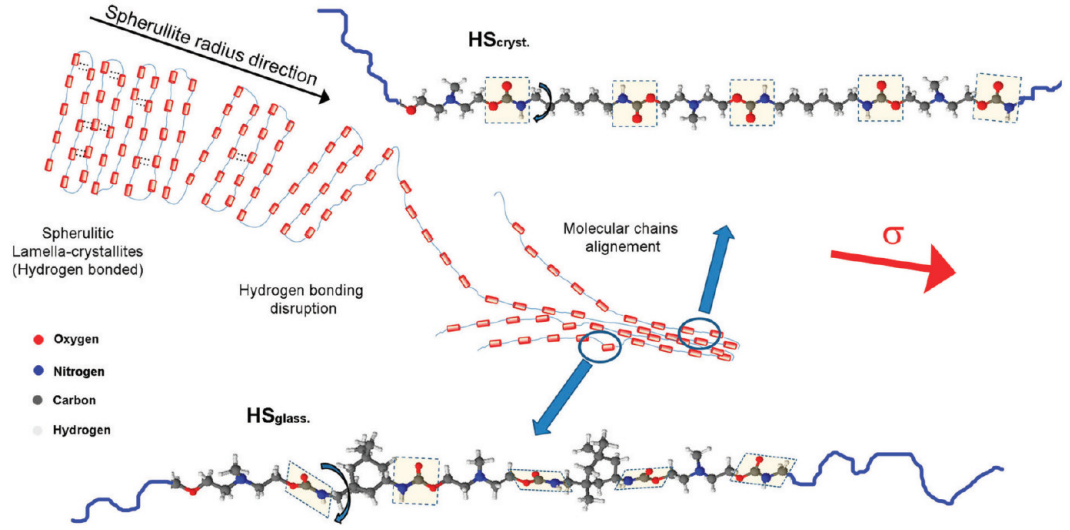

Figure 6. Model for molecular rearrangement of $HS_{glass.}$-$SS_{cryst.}$ and $HS_{cryst.}$-$SS_{cryst.}$ chains upon stretching. Also shown the most stable molecular conformations of $HS_{glass.}$ and $HS_{cryst.}$ segments and the relative positioning of consecutive urethane groups.

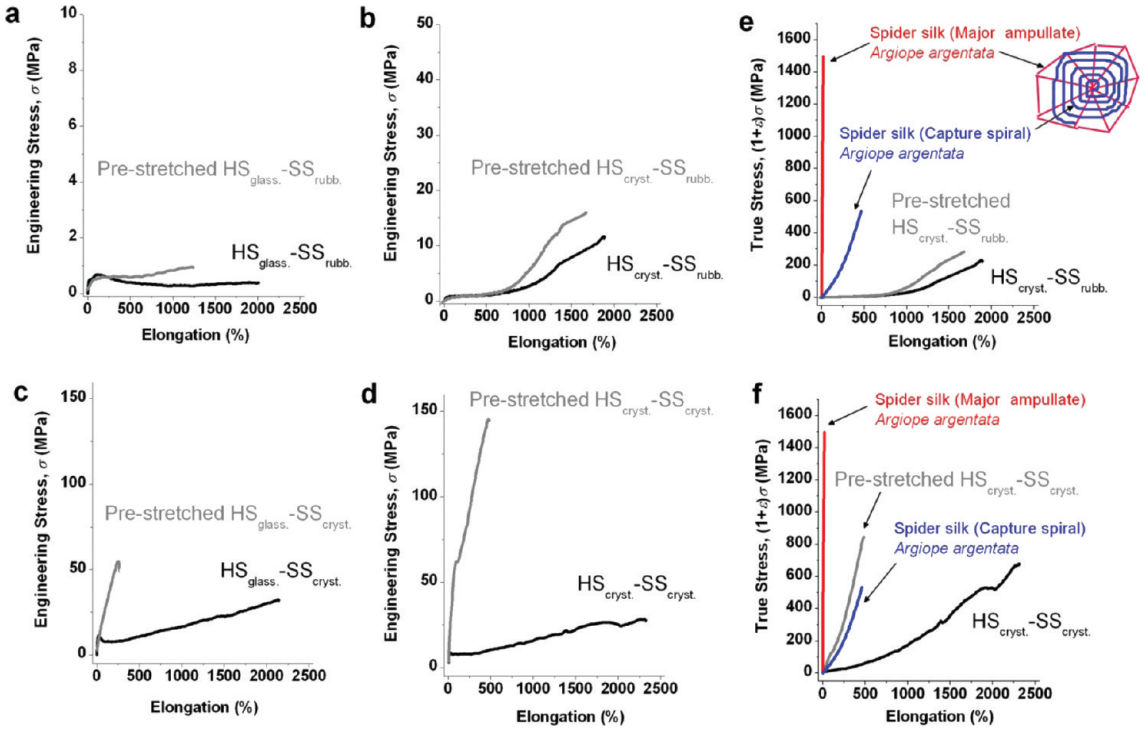

Figure 7. Stress−strain curves of non stretched (black) and prestretched (gray) representative samples of (a) $HS_{glass.}$-SS_{rubb}, (b) $HS_{cryst.}$-SS_{rubb}, (c) $HS_{glass.}$-$SS_{cryst.}$ and (d) $HS_{cryst.}$-$SS_{cryst.}$. In (e) and (f) representative true stress curves of $HS_{cryst.}$-$SS_{rubb.}$ and $HS_{cryst.}$-$SS_{cryst.}$ are plotted along with true stress curves for *Argiope argentata* spider silks.[3] True stress was defined considering a constant samples volume between clamps, as engineering stress (σ) multiplied by $(1 + \varepsilon)$, where ε is the nominal strain (mm mm^{-1}).[26]

Table 2. Resume of the Mechanical Properties of Original and Pre-Drawn Polyurethanes

Polyurethane	E (MPa)	σ_y (MPa)	ε_y (%)	σ_{max} (MPa)	ε_{max} (%)	T (MJ m^{-3})
$HS_{glass.}$-$SS_{rubb.}$	1.3 ± 0.5	0.6 ± 0.1	143 ± 35	0.6 ± 0.1	2500 ± 500	6 ± 2
$HS_{glass.}$-$SS_{rubb.}$-drawn	1.7 ± 0.6	0.7 ± 0.1	90 ± 6	1.5 ± 0.4	1040 ± 170	9 ± 1
$HS_{cryst.}$-$SS_{rubb.}$	2.1 ± 0.3	0.9 ± 0.2	120 ± 45	10.5 ± 3.8	2000 ± 380	75 ± 44
$HS_{cryst.}$-$SS_{rubb.}$-drawn	2.5 ± 0.3	1.2 ± 0.1	78 ± 25	20.4 ± 3.4	1530 ± 460	260 ± 81
$HS_{glass.}$-$SS_{cryst.}$	106.0 ± 27.0	10.6 ± 0.5	21 ± 2	28.4 ± 3.7	2100 ± 190	337 ± 34
$HS_{glass.}$-$SS_{cryst.}$-drawn	44.7 ± 6.9	44.2 ± 10.5	208 ± 41	45.1 ± 10.8	221 ± 41	68 ± 10
$HS_{cryst.}$-$SS_{cryst.}$	61.4 ± 12.0	8.6 ± 0.6	25 ± 6	26.9 ± 2.1	2070 ± 290	350 ± 57
$HS_{cryst.}$-$SS_{cryst.}$-drawn	98.3 ± 14.4	58.8 ± 2.7	95 ± 7	147 ± 14	480 ± 40	425 ± 28

dx.doi.org/10.1021/ma300397e | *Macromolecules* 2012, 45, 3436−3443

linking sites, being the most typical case of PU elastomer.[17] The materials with crystalline SS presented higher modulus and yield stresses, being $HS_{glass.}$-$SS_{cryst.}$ stiffer than $HS_{cryst.}$-$SS_{cryst.}$ but both with similar deformability, ε_{max} and strength, σ_{max}, between them. When prestretching the materials with SS_{rubb}, $HS_{glass.}$-$SS_{rubb.}$ lead to an increase of strength from 0.6 ± 0.1 MPa to 1.5 ± 0.5 MPa while $HS_{cryst.}$-$SS_{rubb.}$ leads to an increase in strength from 10 ± 4 MPa to 20 ± 3 MPa. Variations in mechanical properties of $HS_{glass.}$-$SS_{rubb.}$ were not as significant as variations of $HS_{cryst.}$-$SS_{rubb.}$, especially if we consider the toughness, which varied from 6 ± 2 to 9 ± 1 MJ m^{-3} for the $HS_{glass.}$-$SS_{rubb.}$ and from 75 ± 44 to 260 ± 81 MJ m^{-3} for the $HS_{cryst.}$-$SS_{rubb.}$. This fact was attributed as the aforementioned $HS_{cryst.}$ partial mobility and capability to develop strain induced crystallization. In parallel, prestretching the materials with $SS_{cryst.}$ lead to a stiffening just in the case of $HS_{cryst.}$-$SS_{cryst.}$. In the case of $HS_{glass.}$-$SS_{cryst.}$, despite having a crystalline phase and displaying strain induced anisotropy the elastic modulus decreased respect the nonstretched sample. This is attributed to the disruption of enthalpically driven low energy $HS_{glass.}$ structures upon prestretching, which afterward do not contribute to macromolecular fibrillar organization as $HS_{cryst.}$ does (see Figure 3). In this material the strength was also increased, and this is related to the induced anisotropy and increased overall crystallinity (see Figure 2). In the case of $HS_{cryst.}$-$SS_{cryst.}$ both modulus and strength increased notably (from 59 ± 6 MPa to 98 ± 14 MPa and from 27 ± 2 MPa to 147 ± 14 MPa, respectively). Despite the relatively high modulus and strength for being a thermoplastic, this PU extensibility was as large as 480%. This material presented engineering strengths similar to tendon collagen,[4] but was much more deformable (see Supplementary Table §1). Because of this large deformability a true stress plot was considered convenient in order to account for the cross-section shrinkage occurring during deformation (Figure 7e,f). The combined strength and deformability properties accounted for its remarkable toughness of 425 ± 28 MJ m^{-3} what corresponds to about 2−3 times that of *Araneus diadematus* major ampullate (MA) silk,[3,4,7] about 5−6 times that of *Argiope argentata* capture spiral silk[3] (see Supplementary Table §1), and to authors knowledge the toughest synthetic material reported.

CONCLUSIONS

Four polyurethanes with different segmental nature were synthesized and analyzed mechanically. Mechanical performance of the materials after predrawing was related to their molecular structure. Crystallizable segments resulted to provide higher tensile properties than those based on amorphous segments in spite of these having cyclic nature and bulky groups. In the case of hard segments this has been observed to be due to the capability of semicrystalline hard segments to orient along the stress direction providing macromolecular organization in detriment of hydrogen bonding. Mobility of semicrystalline hard segments allowed transition from spherulitic-lammelar structure to oriented ordered fibrilar organization. Materials combining semicrystalline soft segments with semicrystalline hard segments exhibit relatively high stiffness, great deformability typical from elastomers and high strengths typical of engineered thermoplastics. These combined properties allow proposing this type of engineered PU as materials with potential applicability in different areas like tissue engineering or high loads bearing applications. The molecular design considerations developed in this work pave the way to the future synthesis of new materials with mechanical properties facing traditional confrontations between deformation and strength.

ASSOCIATED CONTENT

Supporting Information

Plots of stress relaxation of polyurethanes, cross-polarized optical microscopy (POM) images of polyurethanes, and morphology variation with strain and a resume of mechanical properties of some high performance fibers and materials. This material is available free of charge via the Internet at http://pubs.acs.org/.

AUTHOR INFORMATION

Corresponding Author

*Telephone: (0034)-943-017185. E-mail: arantxa.eceiza@ehu.es.

Notes

The authors declare no competing financial interest.

ACKNOWLEDGMENTS

B.F.-d'A. acknowledges University of the Basque Country and the (UPV/EHU) postdoc grant "Ayuda a la Especialización de Doctores" for financial support and all authors acknowledge the General Research Services of the University of the Basque Country (SGIker), and especially the *Macroconducta-Mesoestructura-Nanotecnología* unit, for their technical support. Authors also acknowledge funding from the Basque Government through SAIOTEK 10-S-PE10UN22 and SAIOTEK 11-S-PE11UN132 programs and in the frame of *Grupos Consolidados* (IT-365-07).

DEDICATION

This article is dedicated to Proffesor Dr. Iñaki B. Mondragon, who passed away just after his contribution to this work and who founded the research group "Materiales + Tecnologías" (GMT) in 1988. His devotion to science and humanity filled us with lifelong inspiration.

REFERENCES

(1) Simmons, A. H.; Michaes, C. A.; Jelinski, L. W. *Science* **1996**, *271*, 84−87.
(2) Liu, Y.; Shao, Z.; Vollrath, F. *Nat. Mater.* **2005**, *4*, 901−905.
(3) Blackledge, T. A.; Hayashi, C. Y. *J. Exp. Biol.* **2006**, *209*, 2452−2461.
(4) Omenetto, F. G.; Kaplan, D. L. *Science* **2010**, *329*, 528−531.
(5) Agnarsson, I.; Kuntner, M.; Blackledge, T. A. *PLoS ONE* **2010**, *5*, 1−8.
(6) Liu, Y.; Spooner, A.; Porter, D.; Vollrath, F. *Biomacromolecules* **2008**, *9*, 116−121.
(7) Elices, M.; Guinea, G. V.; Plaza, G. R.; Karatzas, C.; Riekel, C.; Agulló-Rueda, F.; Daza, R.; Pérez-Rigueiro, J. *Macromolecules* **2011**, *44*, 1166−1176.
(8) Ritchie, R. O. *Nat. Mater.* **2011**, *10*, 817−822.
(9) Fernández-d'Arlas, B.; Khan, U.; Rueda, L.; Coleman, J. N.; Mondragon, I.; Corcuera, M. A.; Eceiza, A. *Compos. Sci. Technol.* **2011**, *71*, 1030−1038.
(10) Lynd, N. A.; Oyerokun, F. T.; O'Donoghue, D. L.; Handlin, D. L.; Fredrickson, G. H. *Macromolecules* **2010**, *43*, 3479−3486.
(11) Guinea, G. V.; Elices, M.; Pérez-Rigueiro, J.; Plaza, G. R. *J. Exp. Biol.* **2004**, *208*, 25−30.
(12) Ocando, C.; Tercjak, A.; Martín, M. D.; Ramos, J. A.; Campo, M.; Mondragon, I. *Macromolecules* **2009**, *42*, 6215−6224.

(13) Liff, S. M.; Kumar, N.; McKinley, G. H. *Nat. Mater.* **2007**, *6*, 76−83.
(14) Holland, C.; Terry, A. E.; Porter, D.; Vollrath, F. *Nat. Mater.* **2006**, *5*, 870−874.
(15) Lazaris, A.; Arcidiacono, S.; Huang, Y.; Zhou, J. F.; Duguay, F.; Chretien, N.; Welsh, E. A.; Soares, J. W.; Karatzas, C. N. *Science* **2002**, *18*, 472−476.
(16) Fernández-d'Arlas, B.; Rueda, L.; Fernández, R.; Khan, U.; Coleman, J. N.; Mondragon, I.; Eceiza, A. *Soft Mater.* **2011**, *9*, 79−93.
(17) Fernández-d'Arlas, B.; Rueda, L.; de la Caba, K.; Mondragon, I.; Eceiza, A. *Polym. Eng. Sci.* **2008**, *48*, 519−529.
(18) Fernández-d'Arlas, B.; Rueda, L.; Stefani, P. M.; de la Caba, K.; Mondragon, I.; Eceiza, A. *Thermochim. Act.* **2007**, *459*, 94−103.
(19) Waletzko, R. S.; Korley, L. T.; Pate, B. D.; Thomas, E. L.; Hammond, P. T. *Macromolecules* **2009**, *42*, 2041−2053.
(20) Christenson, E. M.; Anderson, J. M.; Hiltner, A.; Baer, E. *Polymer* **2005**, *46*, 11744−11754.
(21) Kijio, K.; Kakamura, S.; Furukawa, M. *Polymer* **2004**, *45*, 8147−8152.
(22) Peterlin, A. In *Man made fibers, science and technology*; Marks, H. F., Atlas, S. M., Cernia, E., Eds.; John Wiley and Sons: New York, 1967; Vol. *1*, pp 283−340.
(23) Melning, V.; Apostu, M. O.; Tura, V.; Ciobanu, C. *J. Membr. Sci.* **2005**, *267*, 58−67.
(24) Papadopoulos, P.; Sölter, J.; Kremer, F. *Eur. Phys. J. E* **2007**, *24*, 193−199.
(25) Fafarman, A. T.; Sigala, P. A.; Herschlag, D.; Boxer, S. G. *J. Am. Chem. Soc.* **2010**, *37*, 12811−12813.
(26) Ward, I. M.; Hadley, D. W. In *An introduction to the mechanical properties of solid polymers*, 1st ed.; John Wiley and Sons: Chichester, England, 1993; pp 213−218.